

Influence of Pitting Corrosion on the Spatial-Time Dependent Reliability of Reinforced Concrete Bridge Girder

Omran Kenshel^{1*}, Mohamed Suleiman¹

¹Assistant Professor, The Department of Civil Engineering, University of Tripoli, Tripoli, Libya

DOI: [10.36347/sjet.2021.v09i11.003](https://doi.org/10.36347/sjet.2021.v09i11.003)

| Received: 03.11.2021 | Accepted: 08.12.2021 | Published: 14.12.2021

*Corresponding author: Omran Kenshel

Abstract

Original Research Article

Estimating the Reliability (Probability of Failure) of Reinforced Concrete (RC) structures in marine environments has been of major concern among researchers in recent years. While General (uniform) corrosion affects the reinforcement by causing a uniform loss of its cross-sectional area, Pitting (localized) corrosion concentrates over small areas of the reinforcement. Many studies have focused on the effect of general corrosion, the effect of pitting corrosion on the structure reliability has not been fully investigated. Furthermore, due to the variability associated with the parameters involved in the reliability estimation of the corroded structure, this paper focuses on the effect of variability of pitting corrosion on the structure reliability. The analysis also takes into consideration the Spatial Variability (SV) of key deterioration parameters often neglected in previous studies. The authors have used their experimental data in modeling SV parameters of a specific deterioration parameter. The analysis adopted here used Monte Carlo (MC) simulation technique to construct a Spatial-Time Dependent model to estimate the girder reliability. The results showed that pitting corrosion potentially has a far more aggressive effect on the structure reliability than general corrosion and that pitting corrosion affects shear resistance far more severely than it would affect flexure resistance. The analysis showed that after 50 years of service, the reduction in the beam reliability due to pitting corrosion was 51% higher than that caused by general corrosion and that considering SV has caused the reliability predicted in terms of pitting corrosion to decrease by 12%. In the case of general corrosion, the decrease in beam reliability was only about 2% for the SV scenario.

Keywords: Pitting corrosion, Reliability, Reinforced concrete, Monte Carlo simulation, Spatial variability.

Copyright © 2021 The Author(s): This is an open-access article distributed under the terms of the Creative Commons Attribution 4.0 International License (CC BY-NC 4.0) which permits unrestricted use, distribution, and reproduction in any medium for non-commercial use provided the original author and source are credited.

1. INTRODUCTION

For Reinforced Concrete (RC) bridge structures located in marine environments, different deterioration mechanisms have been recognized, e.g. carbonation-induced corrosion, freeze/thaw, alkali-silica reaction, sulfate attack, etc. The majority of RC bridge structures in marine environments, however, deteriorate mainly due to chloride-induced corrosion (Mallet, 1994). For RC bridge structures in marine environments affected by localized (pitting) type of corrosion has not been investigated properly in the literature. Therefore, RC bridge structures in marine environments deteriorating due to pitting corrosion will be the focus of this paper. Many models have been proposed by various researchers to describe the deterioration process of RC structures exposed to chloride-induced corrosion. These models are often used by researchers in a probabilistic framework to allow for the inherent variability of the model

parameters to be considered. This can be done by describing each model parameter within the deterioration model as a random variable characterized by its Probability Density Function (PDF). However, by modeling each parameter as a random variable with a specified PDF mean (μ) and standard deviation (σ), the Spatial Variability (SV), i.e. the fluctuation of properties in space, of the model parameters is ignored. It may be accepted that some model parameters, such as the yield strength of the reinforcing steel, would exhibit very little SV due to the high-quality control that is implemented by the manufacturer. However, many material and geometrical properties, e.g. cover depth, concrete compressive strength, are expected to show considerable SV due to the effect of environmental conditions and the inconsistency of the workmanship. It is tabulated that neglecting such sources of uncertainty will have some impact on the evaluated safety performance of the structure. Investigating the

magnitude of this impact on the safety profile of the structure affected by pitting corrosion has been the prime objective of this paper.

2. MATERIAL AND METHODS

The material deterioration models are often described in the literature in the context of structure service life modeling where each stage of the deterioration process is quantified in terms of time and the sum of these times makes the total service life. For RC structures, it is postulated that during the hydration of cement a highly alkaline pore solution (pH between 13 and 13.8), principally of sodium and potassium hydroxides, is gained (Bertolini, 2004). In this alkaline environment a protective oxide layer, a few nanometers thick, is formed on the reinforcing steel bar embedded in concrete. Despite its attested protective property against mechanical damage of the steel surface, the formed layer can be destroyed by the carbonation of concrete or by the presence of chloride ions leading to the depassivation of the reinforcing steel. This stage of the service life of RC structures affected by corrosion-induced deterioration is referred to as the Initiation stage, Figure 1. The second distinguished service life stage begins when the steel reinforcement is depassivated and the corrosion process begins its activity and finishes when an undesired limit state is reached prompting a rehabilitation action to be taken. This stage is referred to as the Propagation Stage.

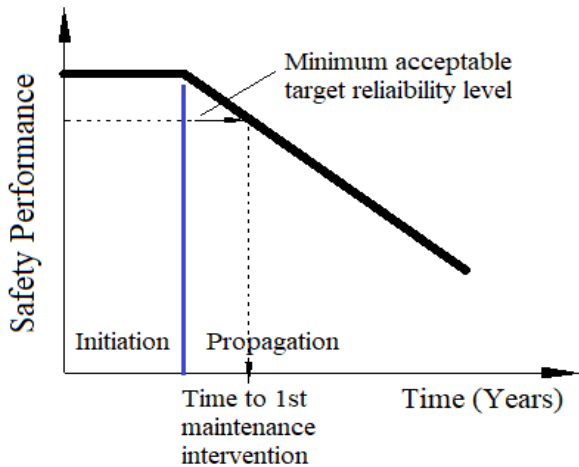


Figure 1: Schematic representation of corrosion-affected structure service life

2.1. The Initiation Stage

The first step towards a practical quantification of the service life of an RC structure exposed to a chloride-rich environment is to predict the time it takes for the chloride ions to penetrate the concrete cover and reach the reinforcement in enough quantity to depassivate the reinforcement and hence initiate corrosion. Traditionally, the time for chloride ions to

penetrate through the concrete cover from the surface and reach a critical (threshold) value C_{cr} at the level of reinforcement, has been modeled using an expression derived from Fick's 2nd law of diffusion.

$$T_i = \frac{C_d^2}{4D_{app}} \left[\left(\operatorname{erf}^{-1} \left[\frac{C_{cr} - C_s}{C_i - C_s} \right] \right)^2 \right] \dots\dots\dots (1)$$

Where T_i is time to corrosion initiation (years); D_{app} is the diffusion coefficient in (mm²/year); C_s is the surface chloride content, C_i is the initial chloride content and C_{cr} is the critical chloride content. C_s , C_i , and C_{cr} are in (Cl% per mass of cement or concrete) and C_d is the reinforcement cover depth in (mm). D_{app} , C_s , and C_i , are often determined by fitting data of chloride concentration obtained from chemical analysis of concrete dust samples taken across the depth of the structure to Fick's 2nd law of diffusion. In this paper, the data on the aforementioned two parameters were obtained from the analysis of 45 concrete cores collected from the Ferrycarrig Bridge located on the southwest of Ireland (O'Connor and Kenshel, 2013).

2.2. The Propagation Stage

As the propagation stage starts, the cross-sectional area of longitudinal reinforcement of the RC beam, which provides its flexural capacity, will be reduced due to the ongoing corrosion activity, leading to rupture at the critical cross-section of the RC beam. Similarly, the shear links, which provide the beam with a substantial proportion of its shear capacity, lose part of its cross-sectional area as corrosion progresses. Consequently, the structural safety of the beam will be reduced over time. In this paper, the structural safety of the considered beam girder is determined concerning the flexural and the shear strengths although other effects (e.g. torsion, fatigue, etc.) can equally be considered.

2.3. Flexure Resistance Models

In AASHTO-LRFD (1994), the computation of the flexural capacity is based on Whitney's rectangular approximation of the parabolic stress distribution shown in Figure 2(a) (Wang and Salmon, 2002). To determine the flexure capacity of an RC T-beam section, two cases have to be considered, case (1) where $a \leq h_f$, Figure 2(b), and case (2); where $a > h_f$, Figure 2(c), (h_f is the flange thickness of the T-beam). To determine if $a \leq h_f$, the distance x shown in Figure 2(a) (the distance from the extreme compression fiber to the neutral axis NA) must be found according to Equation 3.

$$x = \frac{A_s f_y - 0.85 \eta_1 (b_f - b_w) h_f}{0.85 \eta_1 f'_c b_w}; \quad a = \eta_1 x \dots\dots\dots (2)$$

While values for the parameter η_1 are given in Table 1, other parameters are as defined in Table 2.

Table 1: Values for η_1 given in (Barker and Puckett, 1997).

For	η_1
$f'_c \leq 28 \text{ MPa}$	0.85
$f'_c \geq 56 \text{ MPa}$	0.65
$28 \leq f'_c \leq 56 \text{ MPa}$	$0.85 - 0.05(f'_c - 28)/7$

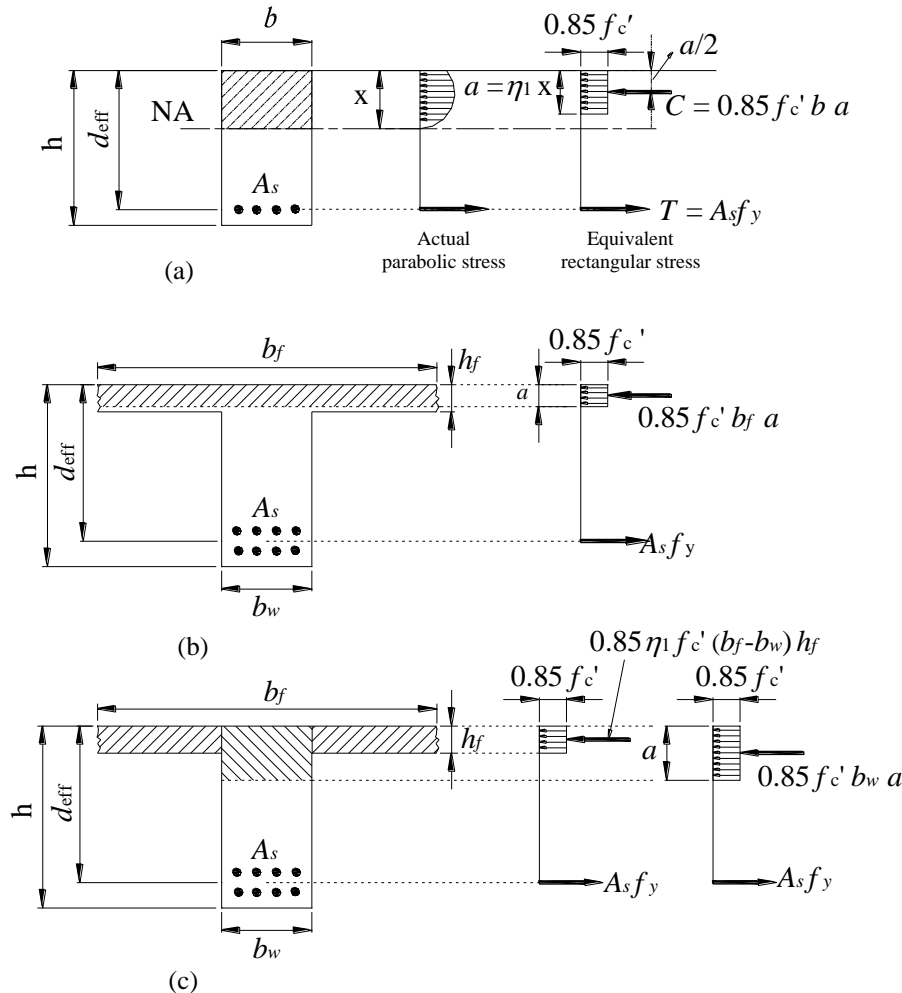


Figure 2: Flexural Capacity of RC T-Beam Section with Tension Reinforcement Only; (a) Forces on The Section for Rectangular RC Section (b) a is in The Flange, (c) a is in The Web After Barker and Puckett (1997)

The computation for the beam flexure capacity at any time (t) of a T-section can be carried out for the two cases (assuming only the reinforcement cross-

sectional area is reducing with time due to the effect of corrosion, no bond loss or anchorage slip is considered as follows:

Case (1): $a \leq h_f$, Figure 2(b).

$$M_u(t) = A_s(t)f_y \left[d_{eff} - \frac{A_s(t)f_y}{2 \times 0.85 f'_c(t) b_f} \right] \dots\dots\dots (3)$$

Case (2): $a > h_f$, Figure 2(c).

$$M_u(t) = [A_s(t)f_y - 0.85 \eta_1 f'_c(t) (b_f - b_w) h_f] \times \left[d_{eff} - \frac{A_s(t)f_y - 0.85 \eta_1 f'_c(t) (b_f - b_w) h_f}{2 \times 0.85 f'_c(t) b_w} \right] + 0.85 \eta_1 f'_c(t) (b_f - b_w) h_f \left(d_{eff} - \frac{h_f}{2} \right) \dots\dots\dots (4)$$

Where all variables involved in the formulation of (4) & (5) are defined in Figure 2 and Tables 1&2.

2.4. Shear Resistance Model

Similarly, the time-dependent ultimate shear resistance of the beam at any given section is calculated

by simply combining the contributions of concrete and shear links to the shear resistance of the section provided by AASHTO-LRFD (1994) as follows:

$$V_u = V_c + V_s \dots\dots\dots (5)$$

$$V_u(t) = \frac{1}{6} \sqrt{f'_c(t)} b_w d_{eff} + \frac{A_v(t) f_y d_{eff}}{s} \dots\dots\dots (6)$$

Where all parameters in (6) & (7) have been defined in Table 2. Equation (7) was derived from an expression that is based on the variable-angle truss model for a uniformly loaded beam in which the beam is treated as a truss with a diagonal crack in which the local stresses at the crack (indicated in Figure 3) must be in equilibrium. In the original derivation of (7) the

vertical forces acting on the diagonally cracked section were set to be in equilibrium, the distance between the tension and the compression reinforcement, d_v , were approximated by d_{eff} and the angle ϕ was taken as $\phi=45^\circ$ whereas V_{ci} was experimentally related to f_c' so that $V_{ci}=1/6\sqrt{f_c'}$ (MPa).

Table 2: Random variables for the RC T-beam girder

Variable (units)	Description	Distribution	Mean (COV)
D_{oM} (mm)	Initial diameter of flexure reinforcement	Lognormal	35.8 (0.02)
D_{oV} (mm)	Initial diameter of shear reinforcement	Lognormal	12.7 (0.02)
$A_s(t)$ (mm)	The time-dependent cross-sectional area of flexure reinforcement	Lognormal	Equations 12 & 17
$A_v(t)$ (mm)	The time-dependent cross-sectional area of shear reinforcement	Lognormal	Equations 12 & 17
d_{eff} (mm)	Effective depth of flexure reinforcement	Lognormal	687 (0.03)
C_{dM1} (mm)	Cover depth of flexure reinforcement (Layer 1)	Lognormal	50 (0.10)
C_{dM2} (mm)	Cover depth of flexure reinforcement (Layer 2)	Lognormal	137 (0.10)
C_{dV} (mm)	Cover depth of shear links	Lognormal	(38.1, 0.10)
b_f (mm)	Effective flange width	Fixed	2600
b_w (mm)	Web width of the beam	Fixed	400
h_f (mm)	Flange thickness	Fixed	190
h_w (mm)	Web height	Fixed	600
S (mm)	Shear links spacing	Lognormal	100 (0.15)
f_y (MPa)	The specified Steel reinforcement yield strength	Lognormal	460 (0.12)
f_{ck}' (MPa)	The specified (characteristic) 28 days concrete compressive strength	Lognormal	40 (0.18)
f_c' (MPa)	Time-dependent compressive strength	Lognormal	Equation 11

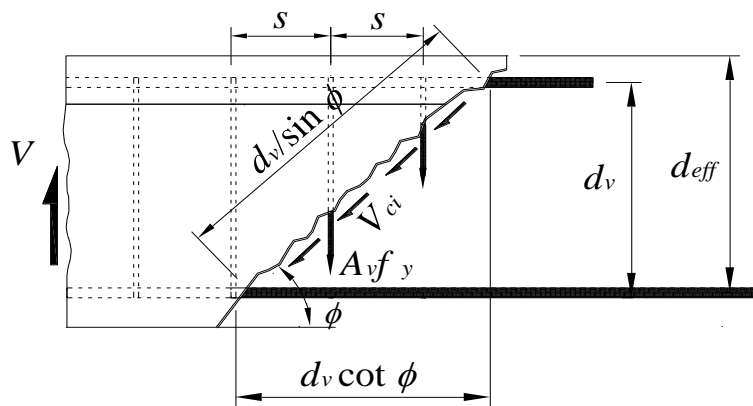


Figure 3: Shear strength of RC section with shear reinforcements after Barker and Puckett (1997)

2.5. Modelling the Concrete Compressive Strength

In design, the characteristic strength (f_{ck}'), rather than the mean strength, is used (i.e. $f_c' = f_{ck}'$ in all previous code-provided equations). This strength is defined as the level below which only a small proportion (usually 5%) of all the results are likely to fall (Narayanan and Beeby, 2001). When concrete is ordered, it is concrete with some specified characteristic strength that will be asked for. To ensure this, the producer has to provide concrete with an average strength that is well above the specified characteristic strength. The amount by which the average exceeds the characteristic value depends on the effectiveness of the producer’s control methods. Euro Code 2 (EC2) relates the concrete mean cylinder compressive strength to the specified characteristic strength for concrete up to 50 MPa as follows:

$$f'_{cyl} = f'_{ck} + 8 \text{ (MPa)} \dots\dots\dots (7)$$

Based on worker performance survey data, Stewart (1997) performed a probabilistic analysis in which he then proposed that the actual concrete compressive strength mean (μ) and coefficient of variation (COV) of the assessed structure may be related to the compressive strengths obtained from the standard test cylinders, which are cured and compacted under standard conditions, as follow:

$$\mu(f'_c) = \mu(k_w) + \mu(f'_{cyl}) \dots\dots\dots (8)$$

$$COV(f'_c) = \sqrt{[COV(k_w)]^2 + [COV(f'_{cyl})]^2} \dots\dots\dots (9)$$

Where (k_w) is a workmanship reduction factor that takes into account the influence of workmanship quality (i.e. curing and compaction) on the actual structure concrete compressive strength and its values

can be obtained from Table 3. The analysis carried out in this paper assumed ‘Fair’ worker performance with ‘minimum of 7 days curing time.

Table 3: Statistical parameters for (k_w) by Stewart (1997)

Worker performance	Minimum curing times			
	3 days		7 days	
	Mean	COV	Mean	COV
Poor	0.53	0.078	0.53	0.078
Fair	0.72	0.078	0.87	0.060
Good	1.0	0	1.0	0

To allow for the influence of the time-dependent increase in concrete compressive strength to be considered in the current analysis, the parameter f_c' , which represents the 28 concrete compressive strength in (4), (5), and (6) can be replaced by a time-dependent compressive strength $f_c'(t)$. The following expression proposed by ACI 209 (1978) has been used in the reliability-based assessment of corroding structures (e.g. Stewart and Mullard, 2007), and therefore it was used here to model the evolution of concrete compressive strength with time.

$$f_c'(t) = \frac{t}{\gamma + \omega t} f_c'(28) \dots\dots\dots (10)$$

Where t is the time elapsed since the beam construction in days, $\gamma=4.0$ and $\omega=0.85$ for moist cured Ordinary Portland Cement (OPC).

2.6. Model Error of the Resistance Models

Based on a study conducted on 1146 RC beams aimed at comparing experimental shear strengths with those obtained from predictive models provided by several national standards and codes (e.g. ACI 318, 1999; AASHTO-LRFD, 1994; BS 8110, 1997 and EN, 2002), Somo and Hong (2006) found that predicting the shear capacity of an RC beam with shear links using (7) may lead to underestimation of the shear capacity of the RC beam. They recommended a model error (bias factor) with a mean value of 1.3 and a coefficient of variation that is larger than 0.3 to account for the uncertainty associated with the use of the predictive model proposed by codes and standards used for estimation of the shear capacity. No similar experimental-based study has been reported in the literature concerning flexure capacity. However, based on the simulation of the moment-curvature relationship performed by Tabsh and Nowak (1991) a mean model error of 1.14 and a coefficient of variation of 0.13 were proposed to account for the uncertainty associated with the flexure resistance model determined according to AASHTO-LRFD (1994).

2.7. Materials Deterioration Models

Models describing the loss in the flexure and shear capacities over time due to the chloride-induced corrosion will be covered in this section. These models are vital for formulating the LS functions which will be

employed to estimate the Probability of Failure (P_f) and hence the Reliability Index (β). Reliability Index (β) is an indication of the performance of the structural safety and is related to the (Pf) through the following expression (Melchers, 1999):

$$\beta = -\Phi^{-1}(P_f) \dots\dots\dots (11)$$

Where $\Phi(\cdot)$ is the standard normal distribution function.

Before proceeding to describe the models used for the determination of the residual flexure and shear capacities of the RC beam due to general and pitting corrosion, the resistance models will be introduced.

2.7.1. Modelling Loss of Reinforcement

In this paper, two forms of corrosion mechanisms were considered for the reduction in the reinforcement cross-sectional area. These are the General corrosion and the Pitting (localized) corrosion. General corrosion affects the reinforcement by causing a uniform loss of its cross-sectional area. Pitting corrosion, in contrast to general corrosion, concentrates over small areas of the reinforcement. The calculation of the residual cross-sectional area of the reinforcement due to any of the two types of corrosion will be explained here.

2.7.1.1. Due to General Corrosion

If the corrosion is assumed to be of a uniform type, often referred to as ‘General corrosion’, Figure 4(a), the loss of reinforcement diameter can be described by the use of Faraday’s law of electrochemical equivalence (Andrade and Alonso, 1996). Faraday’s law indicates that a constant corrosion rate of 1.0 $\mu\text{A}/\text{cm}^2$ corresponds to a uniform metal loss of bar diameter of 0.0232 mm per year (or 1.0 $\mu\text{A}/\text{cm}^2=11.6 \mu\text{m}/\text{year}$ metal loss of the bar radial). If the corrosion rate is assumed to be constant over time, then the remaining cross-sectional area of corroding main reinforcement after t-years $A_s(t)$ can thus be estimated as:

$$A_s(t) = \sum_1^{n_b} \frac{\pi[D_o - \Delta D(t)]^2}{4} \geq 0 \dots\dots\dots (12)$$

$$\Delta D(t) = 0.0232 i_{corr} (t - T_i) \dots\dots\dots (13)$$

2.7.1.2. Due to pitting corrosion

Pitting (localized) corrosion is a very intense form of corrosion in which a small area over the reinforcement length may suffer a much greater loss of section than the rest of the reinforcing bar. For that reason, the measurements of the corrosion rate (i_{corr}) cannot be directly translated into the loss of cross-sectional area of the corroding bar in the same way indicated by (13). According to Gonzalez *et al.*, (1995), the maximum penetration depth caused by pitting corrosion (P_{max}) can be 4 to 8 times that caused by general corrosion. This conclusion was derived from results obtained from tests made on specimens 125 mm long and have a bar diameter of 8 mm. The corrosion

rate i_{corr} for general corrosion can be related to P_{max} at any time t via the ratio $R = P_{max}/P_{av}$, where P_{av} is the average penetration depth expected from general corrosion ($P_{av} = \Delta D/2$). Therefore, the maximum pitting depth in (mm) at any time may be estimated as follows (Gonzalez *et al.*, 1995):

$$P_{max}(t) = 0.0116i_{corr}(t - T_i)R \dots\dots\dots (14)$$

Where T_i is the time to corrosion initiation (years), n_b is the total number of reinforcing bars, and D_o is the original bar diameter and $\Delta D(t)$ is the reduction of bar diameter at the time, t .

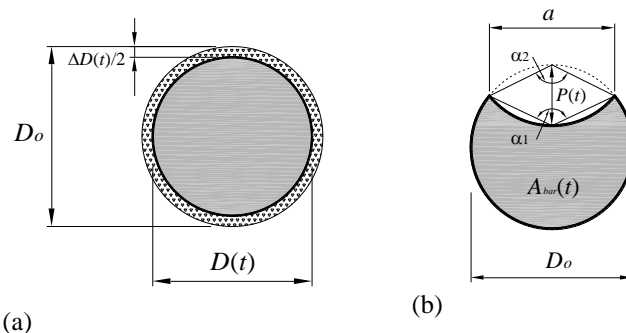


Figure 4: (a) General corrosion, (b) Pitting corrosion configuration according to Val and Melcher (1997)

The residual cross-sectional area of a single corroding bar at any time t can be calculated by assuming a pit shape, Val and Melcher (1997) assumed the pit configuration shown in Figure 4(b) and calculated the residual cross-sectional area as follows:

$$A_{bar}(t) = \begin{cases} \frac{\pi D_o^2}{4} - A_1 - A_2 \text{ for } P(t) \leq \frac{D_o}{\sqrt{2}} \\ A_1 - A_2 \text{ for } \frac{D_o}{\sqrt{2}} < P(t) \leq D_o \\ 0 \text{ for } P(t) > D_o \end{cases} \dots\dots\dots (15)$$

Where:

$$\left. \begin{aligned} A_2 &= \frac{1}{2} \left[\alpha_2 P(t)^2 - a \frac{P(t)^2}{D_o} \right] \\ a &= 2P(t) \sqrt{1 - [P(t)/D_o]^2} \\ \alpha_1 &= 2\arcsin(a/D_o) \\ \alpha_2 &= 2\arcsin(a/2P(t)) \end{aligned} \right\} \dots\dots\dots (16)$$

Finally, the remaining total cross-sectional area of the reinforcement subjected to pitting corrosion, after $(t-T_i)$ years of active corrosion, $A_s(t)$ can be estimated as follows:

$$A_s(t) = \sum_{j=1}^{n_b} A_{bar(j)}(t) \geq 0 \dots\dots\dots (17)$$

Where n_b is the total number of longitudinal reinforcement bars.

2.7.2. Modelling the Corrosion Rate (i_{corr})

As can be seen from the relations given in the previous section, the corrosion rate is a key parameter for determining the residual cross-sectional area of both, the flexure and shear reinforcements and hence

the residual capacity of the deteriorating structural member. Usually, i_{corr} is governed by the availability of water and oxygen at the steel-concrete interface, the concrete quality, cover depth, temperature, and humidity (Vu and Stewart, 2000). Considering the importance of i_{corr} as the key parameter which can influence the rate by which the reinforcements cross-sectional area is reduced, several attempts have been made to predict the corrosion rate where field data on the parameter are not available. In this regard, for a typical environment of an ambient relative humidity of 75% and temperature of 20 C°, Vu and Stewart (2000) suggested an empirical formula for the estimation of corrosion rate at the start of the corrosion activity $i_{corr(1)}$. The proposed model relates the corrosion rate to water/cement ratio (wc) and the cover depth (C_d) as follows:

$$i_{corr(1)} = \frac{37.8(1-wc)^{-1.64}}{C_d} \dots\dots\dots (18)$$

In a real case assessment, values of i_{corr} should be obtained from site-specific measurements taken from the structure that is under investigation. However, in many cases, as in this paper, field data on i_{corr} measurements may not be available, therefore, an empirical model such as that proposed above can be used to estimate the i_{corr} for a given structure with a set of environmental conditions and material properties. According to Duprat (2007), results obtained from (19) were found to agree with corrosion rate measurements obtained from experiments performed by Gonzalez *et al.*, (1995) and with the average corrosion rate field measurements suggested by other researchers.

Therefore, in this paper, the empirical corrosion rate model proposed above by Vu and Stewart (2000) was used to produce values of i_{corr} .

Meanwhile, there is strong evidence to suggest that corrosion rate reduces over time as suggested by Liu and Weyers (1998) due to the formation of rust products which slow down the diffusion of irons away from the steel surface. To account for the time-dependent reduction of the corrosion rate, Vu and Stewart (2000) suggested that corrosion rate values obtained from (19) can be modified so that the corrosion rate time-dependent can be obtained as follows:

$$i_{corr(t)} = i_{corr(1)}[\alpha_{cp}(t - T_i)^{\lambda_{cp}}] \dots\dots\dots (19)$$

Where $(t - T_i) \geq 1.0$ year, α_{cp} and λ_{cp} are constants for describing the reduction of the corrosion rate with time their proposed values are 0.85 and -0.3 respectively. The corrosion rate model described above has been used by several other researchers to predict the lifetime safety performance of RC structures (Duprat, 2007; Stewart and Mullard, 2007; Val, 2007; Stewart and Suo, 2009).

In a real case assessment, values of i_{corr} should be obtained from the investigated structure. However, in many cases, as in this research, field data on i_{corr} measurements may not be available, therefore, (19) and (20) may be used to estimate the i_{corr} for a given structure with a set of environmental conditions and material properties. In this paper, Vu and Stewart's (2000) corrosion rate model was used to produce values of i_{corr} that correlate well with the concrete quality and the chosen cover depth used for the considered structure. Care will have to be taken when employing (19) and (20) so that produced values of i_{corr} correspond well with the commonly field-measured i_{corr} data reported in the literature.

3. Spatial Variability Modelling

In a classical reliability analysis problem, material and geometrical properties within a structural component were often treated as homogeneous (perfectly correlated) (e.g. Val and Melchers, 1997; Val

et al., 1998; Frangopol *et al.*, 2001; Duprat, 2007) or randomly distributed (spatially uncorrelated). However, in reality, such properties usually exhibit some limited spatial correlation, Figure 5. That is to say, two samples taken very close to each other can have highly correlated properties and as the distance separating the two samples is increased, the correlation of their properties will decrease. Once the essential characteristics of such fluctuation are obtained, the uncertainty associated with spatial variability of the property of interest (i.e. concrete compressive strength, cover depth, etc.) can be accounted for by dividing the structure surface into several small elements (Vu and Stewart, 2005). Each element will be assigned a value for each of the modeled properties so that the correlation between different elements will depend on the distance separating them. The size of each element (hence the number of elements) will depend on the intensity of the spatial fluctuation of the modeled property.

To demonstrate how SV modeling is carried out, a hypothetical RC beam was used in this study, details of the RC beam adopted here were taken from Enright and Frangopol (1998). The RC beam is a part of a highway bridge located near Pueblo, Colorado, and is designated as ‘Colorado Highway Bridge L-18-BG’. The bridge consists of three 9.1 m simply supported spans where each span has five girders @ 2.6 m centers. The cross-section of the beam girder is shown in Figure 6(a). In this paper, the considered beam girder was assumed to be subjected to chloride ions penetration from all three exposed surfaces as indicated in Figure 6(b). As indicated earlier, in SV modeling, material and geometrical properties are considered not to be perfectly correlated (i.e. spatially constant) within a structure or a component, but rather vary across the structure with some limited field correlation. For this spatial variation to be considered, the structure needs to be divided into many small square/rectangular elements so values for the random variables can be assigned for each element with a correlation between the elements taken into account during the random variables generation process.

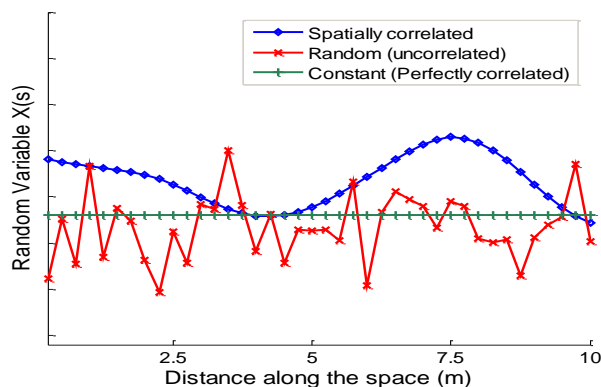


Figure 5: Schematic representation of SV of a physical property

3.1. Structural Discretization

In the beam girder under consideration, for the two vertical sides of the beam, a Two-Dimensional SV model that would take into account the fluctuation of the random variables in both directions can be used. If the fluctuation of random variables in one direction of the beam (e.g. the transverse direction) can be neglected compared with the longitudinal direction, a simple One-Dimensional SV model can be applied. In the current case, in the One-Dimensional SV model, the beam is discretized into strips (rectangular elements) of a width Δ_x (m) and a height that is equal to the height of the

beam web (h_w) as shown in Figure 7(a). In the Two-Dimensional SV model, the vertical faces of the beam were divided into multiple equal segments with a vertical size $\Delta_y = h_w/k_y$ (m) where k_y is the number of SV elements specified for the vertical direction, Figure 7(b). The same meshing principle could be applied to the bottom face of the beam; however, due to the relatively smaller width of the beam bottom ($b_w=0.4$ m) as compared with the length of the beam (9.6 m), only a One-Dimensional meshing model was considered for the bottom face Figure 7(c). Determining the size of the SV elements will be discussed in the following section.

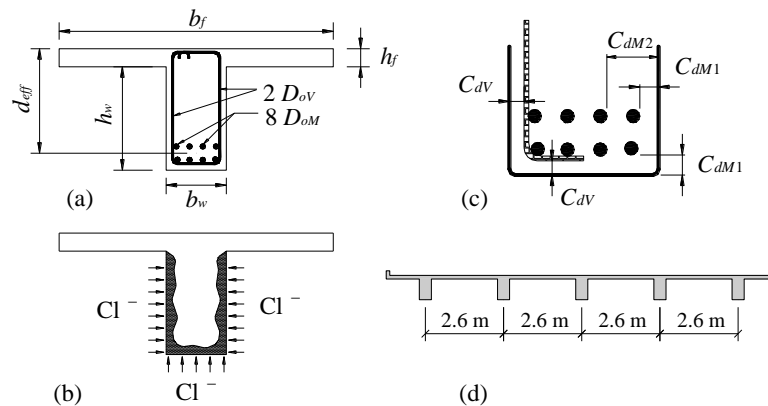


Figure 6: (a) Reinforced Concrete Beam Cross-Section, (b) Chloride Attack, (c) Reinforcement Details, (d) Girder Spacing

3.2. Size of the VS Elements

The size of the discretized SV element to be chosen depends on the parameter θ of the random variable of interest and the correlation coefficients between the two neighboring elements calculated using the autocorrelation function. If the size of the SV element is too large, this implies that the random variable is constant within each element which may result in underestimation of the effect of spatial variability of the random variable particularly when the value of θ is too small relative to the SV element size. On the other hand, a small element size leads to the generation of a very fine mesh that causes the random variables in elements close to each other to have a high correlation with each other resulting in numerical difficulties in the decomposition of the correlation coefficient matrix. Interested readers are referred to reference (Kenshel, 2009) for more details on this issue. Therefore, the SV element size has to be chosen in such a way as to avoid high correlations among the random variables specified for neighboring elements. The available literature has recommended that the element size should be between $\theta/4$ and $\theta/2$. A sensitivity analysis was performed by the first author to define the optimal element size for the beam example under consideration. The optimal element size, in this case, was found to be $\Delta_x = 0.31$ m for the One-dimensional SV model which corresponds to using 31 elements for the beam.

3.3. The Autocorrelation Function

The autocorrelation function $\rho(\tau)$ is a mathematical expression needed to specify the correlation behavior between observations as a function of the separating distance (i.e. between any two neighboring SV elements separated by distance, τ). The role of the autocorrelation function in SV modeling is explained in detail by the author (Kenshel, 2009). Several autocorrelation functions have been proposed in the literature to choose from (Vanmarcke, 1983). To date, no specific autocorrelation function has been favored for the type of analysis that is similar to the one carried out in this study. However, the Square Exponential autocorrelation function is the most frequently used by researchers in the field of RC corrosion (Li et al., 2004; Malioka and Faber, 2004; Vu and Stewart, 2005) and therefore was used in the current paper to generate the correlated data for each SV element. The Two-Dimensional form of the Square Exponential autocorrelation function is expressed as follows:

$$\rho(\tau) = \exp \left[- \left(\frac{|\tau_x|}{d_x} \right)^2 - \left(\frac{|\tau_y|}{d_y} \right)^2 \right] \dots \dots \dots (20)$$

Where d_x and d_y are the model parameters (correlation lengths) for a Two-Dimensional SV in x and y direction respectively which is related to the scale of the fluctuation, θ , through the relation $\theta = \sqrt{\pi d}$, and $\tau_x = x_{(j+1)} - x_j$, $\tau_y = y_{(j+1)} - y_j$ are the distances between the center of elements j and $j+1$ in x and y directions

respectively. If a One-Dimensional SV model is considered the y component is neglected.

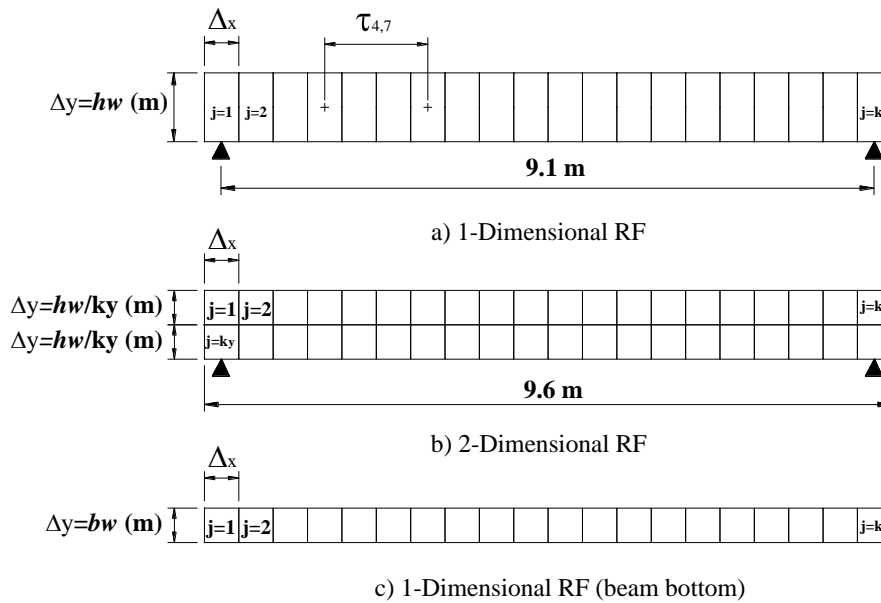


Figure 7: Discretization of the beam into *k* number of SV elements

It can be observed from (21) that the degree of correlation between the SV elements is dependent upon two main parameters; the correlation length (*d*), hence θ , and the distance (τ) which is directly dependent on the element size Δ_x and Δ_y . To obtain a suitable value of *d* for any SV variable (i.e. a random variable that is also a spatially variable), data sets consisting of sample measurements taken at frequent distances are needed. In practice, such measurements are rarely taken at frequent distances; consequently, data on *d* are scarce and usually assumed based on engineering judgment. However, in the current study values for the parameter *d* for two key deteriorating variables, namely C_s and D_{app} , were obtained following extensive experimental and numerical/statistical analysis carried by the author (Kenshel, 2009). The values of the parameter *d* were determined for both variables by performing spatial

correlation analysis on the data collected from the aging RC Ferrycarrig Bridge (O'Connor & Kenshel, 2013).

Based on the spatial correlation analysis performed by the first author in (Kenshel, 2009), values of *d* (hence θ) were found to be as indicated in Table 4. Due to the positive correlation between D_{app} and other concrete properties such as f'_c , w_c , and $i_{corr(1)}$, it was reasonable to assume that these later variables have similar fluctuation properties as that of their associated variable, D_{app} . Therefore, all variables which are dependent on or related to D_{app} were assumed to have the same θ value as that found for D_{app} . For all other SV variables, values of θ that have been used by other researchers in the field (e.g. Li et al., 2004; Vu and Stewart, 2005) indicated in Table 4 were used.

Table 4: The Scale of Fluctuation (θ) and The Corresponding Correlation Length (*d*) to be Used in The Analysis

Variable	θ (m)	<i>d</i> (m)	Reference
C_s	2.7	1.5	Kenshel, (2009)
$D_{app}, f'_c, w_c, i_{corr(1)}$	1.9	1.1	Kenshel, (2009)
Other variables	3.5	2.0	Li et al., (2004) & Vu and Stewart (2005)

3.4. Modelling SV of Pitting Corrosion

For SV modeling of pitting corrosion, the maximum pitting depths was specified through the use of the factor *R* which relates the maximum pitting depth to the average penetration caused by the general corrosion. The analysis carried out in this paper assumes statistical independence between the pitting depths for each SV element and between reinforcing bars within the same SV element. The concept of

having fully correlated or independent pitting depths is illustrated in Figure 8. In the first case, (a) fully correlated, for the same MC realization; all corrosion-induced pits would have the same depth. In the second case, (b) independent, total independency between pits depths was assumed resulting in different pitting depths to be generated for each reinforcing bar within the same SV element or the same bar expanding across different elements.

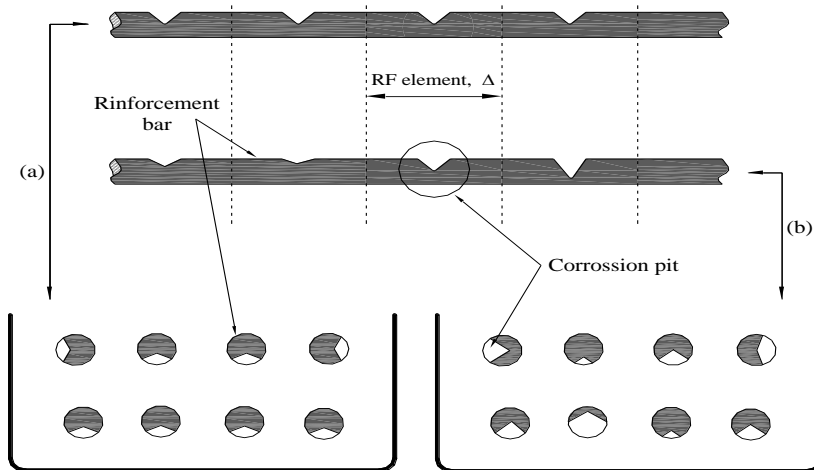


Figure 8: A single reinforcing bar and beam cross-section shows (a) Fully correlated and (b) Independent corrosion-induced pitting depths

In reality, there may exist some correlation between the pitting depths of the neighboring reinforcing bars or between the pitting depths of the same bar. Although it is highly unlikely that all corrosion-induced pits would have the same depth value (i.e. fully correlated pitting depths) at the same stage of the corrosion activity, initial results indicated that the time-dependent loss of cross-sectional area due to pitting corrosion was not affected by modeling pitting depths as fully correlated or independent. Therefore, and due to the lack of statistical data to describe the likely correlation between pitting depths, the pitting factors (hence pitting depths) were randomly (independently) generated from the Gumbel distribution as described in (kenshel, 2009).

3.4. Generation of Random Variables for SV Modelling

When a simulation technique is used, the non-correlated standard Gaussian field is obtained through a procedure consisting of two steps:

1. Random numbers uniformly distributed between 0 and 1 are generated and stored in a vector U. (Note that the number of elements of vector U is equal to the number of SV elements).
2. In the second step, the non-correlated standard Gaussian field is obtained with:

$$Y = \Phi^{-1}(U) \dots\dots\dots (21)$$

Where $\Phi(\cdot)$ is the standard normal distribution function. The randomly generated variables (vector Y) are non-correlated; therefore, they need to be transformed in such a way so that the resulting vector possesses a certain correlation between its elements. The procedure for generating spatially correlated random variables, which is summarized in Figure 9, is described in full detail (Kenshel, 2009).

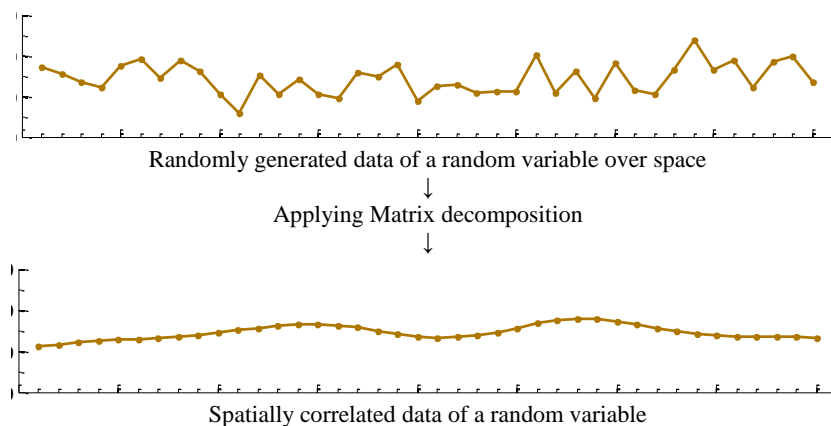


Figure 9. Simplified procedure of generating SV variables

4. Reliability Model (Safety Profile)

To illustrate how SV is expected to influence the safety profile (i.e. the lifetime safety deterioration) of the RC beam under consideration, two cases were

considered. In the first case, the deterioration properties were assumed to be constant along the beam which is equivalent to the state of Perfect Spatial Correlation (i.e. $d \approx \infty$). This is also similar to the conventional

structural reliability analysis which tends to evaluate the failure probability (P_f) of the Limit State (LS) only at sections within the structure where the highest load effect is expected. For example, for a simply supported beam, these sections are the mid-span for the flexure LS and the end support for the shear LS. In this way, SV is ignored and P_f is determined based on evaluating the LS functions at a single SV element located at what is deemed to be the critical section.

In the second case, the SV of the deteriorating properties along the beam was considered, this is the state of Spatial Correlation. Each SV element was considered as an individual component and its individual P_f was used to form a system reliability problem for the whole beam. In this case, the governing LS was not always violated at sections (i.e. center of SV element) within the structure where the highest load effect is induced as mentioned earlier. Other sections along the beam may experience the LS violation first as will be shown later.

4.1. Formulation of the (LS) Function

To calculate the annual failure probabilities (P_f) of the beam under consideration and hence its safety profile, a limit state function (LS), which depends on a set of basic random variables, in terms of each failure mode needs to be formulated and evaluated at the center of each SV element. Two LS functions were considered for the beam problem at hand; the Flexure and the Shear limit states.

4.1.1. Flexure Failure LS

The corresponding LS function for beam failure in flexure at any given time (t) during the service life of the beam $G_M(t)$ is as follows:

$$G_M(t) \leq 0 ; G_M(t) = M_u(t) - M_b(t) \dots\dots\dots (22)$$

Where $M_u(t)$ is the ultimate bending moment capacity of the RC section at time t (years) and can be calculated according to the relevant design code. In this paper $M_u(t)$ is estimated from (4) or (5). $M_b(t)$ is the induced bending moment at the same section in the same year and it will be estimated later in the upcoming section.

4.1.2. Shear Failure LS

The corresponding LS function for beam failure in shear at any given time (t) during the service life of the beam $G_V(t)$ is as follows:

$$G_V(t) \leq 0 ; G_V(t) = V_u(t) - V_b(t) \dots\dots\dots (23)$$

Where $V_u(t)$ is the ultimate shear capacity of the RC section at time t (years) and can be calculated according to the relevant design code. In this paper, $V_u(t)$ is estimated from (6) and (7). $V_b(t)$ is the induced shear force at the same section (element) in the same year (t) and will be estimated from the following section.

4.2. Load Modelling

In previous studies, the load models used to assess the load-carrying capacity of corroding structures were either oversimplified or estimated from conservative standards or codes of practices and not from actual traffic data. In this paper, the load model used was based on realistic site-specific load data acquired by the second author using Weigh in Motion (WIM) technique (O'Connor 2001). In the process, the desired amount of traffic data is generated from the available WIM record. The resulting load effect data, i.e. bending moment and shear force, is obtained using the influence lines procedure. The calculated bending moments and shear forces are then fitted to an Extreme Value (EV) distribution such as Gumbel Type I distribution or Weibull distribution using probability paper. The selection of the appropriate distribution is based upon the linearity of the data plotted. In the present study, Monte Carlo (MC) simulation, a method to be discussed in the following section, was carried out to generate 4 weeks of traffic data, based on the information provided by the 7 days WIM record provided in (O'Connor 2001). The data obtained from the simulation were extrapolated to determine the extreme load effects for the desired reference period of 100 years (i.e. the bridge design life). For further details on this subject the reader is referred to (Kenshel, 2009). The maximum load effect results for different return periods for moment and shear were summarized in Table 5.

Values in this table represent $M_b(t)$ and $V_b(t)$ were used for the evaluation of LS functions expressed in (21) and (22) depending on the remaining service life (reference period) of the structure under consideration. In this paper, the beam girder was evaluated for 100 years (i.e. the expected service life of nowadays bridges), therefor values of $M_b=2062$ kN.m and $V_b=453$ kN were used.

Table 5: The maximum load effect results obtained from the simulated data fitted to Weibull distribution and extrapolated for different reference periods (Kenshel, 2009)

Reference Period (years)	Maximum Bending Moment (kN.m)	Maximum Shear Force (kN)
25	1975	434
50	1993	438
75	2027	446
100	2062	453

4.3. Girder Distribution Factors (GDF)

Having determined the maximum load effect for the desired return period, the value of the moment/shear obtained from the extrapolation does not represent the maximum bending moment/shear acting on a single RC beam girder; this value thus far represents the predicted maximum moment/shear induced by the presence of the heaviest trucks on the bridge deck as a whole in the longitudinal direction.

The proportion of this value that is resisted by a single RC beam girder can be determined by multiplying the obtained value by a specified GDF. In the current study, GDFs for the interior girders were calculated following formulas provided by AASHTO-LRFD (1994). For the beam girder example under consideration, the mean values for the GDFs were calculated for the two loading cases (multiple and a single lane loading) and the result is presented in the following table:

Table 6: Girder distribution factors (GDF)

	Loading scenario	Calculated GDF
Flexure	Two lanes loaded	0.761
	One lane loaded	0.558
Shear	Two lanes loaded	0.866
	One lane loaded	0.702

Based on field testing and finite element analysis, Eom and Nowak (2001) suggested that for simply supported bridges the AASHTO-LRFD GDFs for one lane loading is more realistic for estimating the design load effect. The uncertainty in the GDFs may be expressed in terms of the model error (bias factor). For GDFs based on simplified code methods such as that provided by AASHTO-LRFD (1994), a normally distributed bias factor with a mean value of 0.93 and coefficient of variation of 0.12 was reported in the literature for the case of bending (Nowak *et al.*, 2001). No such information was reported concerning GDF for shear, therefore, the bias factor's mean and coefficient variation for the bending moment GDF's are assumed to be valid for the case of shear.

4.4. Monte Carlo (MC) Simulation

MC simulation is a technique that involves random sampling of variables to artificially produce a large number of experiments (or solutions of an algebraic equation) and observes the results. In the context of structural reliability analysis, this means, each basic random variable is randomly sampled from a specified PDF (Normal, Lognormal, Gumbel, etc.). The LS function $G(X)$ is then checked; if the LS is violated (i.e. $G(X) \leq 0$), then the system has failed. The experiment is repeated many times, each time with a randomly chosen vector of values for the involved basic random variables. If N trials are performed, the probability of failure is approximated by:

$$P_f = \frac{n[G(X) \leq 0]}{N} \dots\dots\dots (24)$$

Where the expression $n[G(X) \leq 0]$ denotes the number of trials n for which $G(X) \leq 0$.

The ability of (25) to accurately estimate P_f depends on the number of simulations N . Theoretically, the estimated P_f will reach the true value as $N \rightarrow \infty$. However, the number of simulations N that can be performed will be limited by the speed of the computer processor that is used. It has been reported (e.g. by Haldar and Mahadevan, 2000) that the P_f obtained using

MC simulation is almost the same as that obtained from another analytical method such as the First Order Reliability Method (FORM) when the number of simulations is relatively large. One has to accept that there should be a 'Trade-off' between the accuracy desired and the time it takes for the computational problem to be solved.

4.5. Calculation of the Reliability Index (β)

Having defined the individual LS functions and assigned the probability distribution to the set of basic random variables and the correlation coefficients between the SV elements, the failure probability for each element for each failure mode can be determined for each year of the structure service life. It has to be noted that when calculating Pf for each period over the service life of the structure, the discretized periods have to be long enough for the correlation between periods to be negligible (Durprat, 2007). For example, Durprat (2007) mentioned that for an industrial warehouse loading, the length of independent periods can be estimated at 2 years. Structural assessments of bridges are often based on a limited reference period of 2-5 years and after the end of this period, the bridge is normally re-assessed as its structural capacity is likely to change (Vu and Stewart, 2000). Thus, it would be more logical and appropriate to compare probabilities of failure for relatively short reference periods. However, too short discretized periods, i.e. one year long, can result in a very long computational time. Therefore, in the present study, due to the lack of reliable data on the correlation between incremental periods, and for the sake of simplicity, the probability of failure will be assumed independent for each incremental period of 5 years which is within the figures indicated by Vu and Stewart (2000). The procedure followed in this study to calculate the time-dependent reliability (Safety Profile) of the beam girder under investigation is as follows:

For a series reliability system consisting of (k) SV elements, the critical limit state occurs when the actual load effects exceed the resistance at the center of any element. The critical moment and shear limit state for a

One-Dimensional RF model consisting of k elements at any year (t_i) can be expressed as follows:

$$G_{t_i}^M(X) = \min_{j=1,k} [R_j^M(t_i) - S_j^M(t_i)] \dots\dots\dots (25)$$

$$G_{t_i}^V(X) = \min_{j=1,k} [R_j^V(t_i) - S_j^V(t_i)] \dots\dots\dots (26)$$

Where $G_{t_i}^M(X)$ and $G_{t_i}^V(X)$ are the flexure and shear LS functions respectively, $R_j^M(t_i)$ and $R_j^V(t_i)$ are the distribution for moment and shear resistance respectively, for element j evaluated at its center at time t_i , $S_j^M(t_i)$ and $S_j^V(t_i)$ are the corresponding load effects at the center of the same SV element due to the load acting at the same time t_i .

The annual probability of failure of the beam in terms of Flexure or Shear can be computed respectively as follows:

$$P_f(i) = \Pr[G_{t_i}^M(X) \leq 0] \dots\dots\dots (27)$$

$$P_f(i) = \Pr[G_{t_i}^V(X) \leq 0] \dots\dots\dots (28)$$

The total annual probability of failure of the beam can then be calculated by combining the beam probability of failure in terms of moment and shear.

$$P_f(i) = \Pr[G_{t_i}^M(X) \leq 0 \cup G_{t_i}^V(X) \leq 0] \dots\dots\dots (29)$$

In general, and as indicated by Stewart (2004), if it is assumed that (m) load events S_j occur within the time interval ($0, T$) at times where $i=1,2,3,\dots,m$, the cumulative probability of failure any time during the time interval from 0 to T for (m) events is:

$$P_f(T) = 1 - \Pr[G_{t_1}(X) > 0 \cap G_{t_2}(X) > 0 \cap \dots \cap G_{t_m}(X) > 0] \dots\dots\dots (30)$$

Where:

$$\Pr[G_{t_i}(X) > 0] = 1 - P_f(i) \dots\dots\dots (31)$$

If the failure events are assumed independent events, then (31) can be approximated by:

$$P_f(T) = 1 - \prod_{i=1}^n [1 - P_f(i)] \dots\dots\dots (32)$$

Where $P_f(i)$ is obtained from (30).

The reliability of the structure is then assessed by using the conditional probability of failure which integrates the survival period of the structure before the time at which the reliability is estimated (Vu and Stewart, 2000; Duprat, 2007). To calculate the conditional probability that the beam will fail in t subsequent years given that it has survived T earlier years, the following expression can be used:

$$P_f^c(t|T) = \frac{[P_f(T+t) - P_f(T)]}{1 - P_f(T)} \dots\dots\dots (33)$$

Where $P_f(T+t)$ and $P_f(T)$ are calculated using (31).

Finally, the probability of failure can then be translated into the Reliability Index (β) through the relationship given in (12).

4.6. Target Reliability (β_T)

In performing a structural safety or reliability assessment the computed reliability index is compared to a target value (β_T), for the considered limit state, and consequence, to determine compliance or violation. Table 7 presents acceptable β_T values as specified by the Eurocode (EN1990-2002). More information on the reliability classes specified by the Eurocode is available in the cited literature.

Table 7: Minimum acceptable safety levels specified by Eurocodes (EN1990-2002)

Reliability Class	Minimum acceptable β_T values (associated p_f)	
	1 year reference period	50 year reference period
CC3 (RC3)	5.2 (1.0×10^{-7})	4.3 (8.5×10^{-6})
CC2 (RC2)	4.7 (1.3×10^{-6})	3.8 (7.2×10^{-5})
CC1 (RC1)	4.2 (1.3×10^{-5})	3.3 (4.8×10^{-4})

5. Important Assumptions

- The random variables are considered constant for a single SV element and each random variable is represented by a value that is evaluated at the center of that element; this means that when corrosion is initiated in an SV element all reinforcing bars in the same layer in that element are assumed to start corroding at the same time.
- After corrosion-induced concrete cracking has taken place, the beam section is still assumed to be physically sound when evaluating the section moment and shear capacities, and only corrosion-induced reduction of the reinforcement cross-sectional area is taken into account. In addition, the bond strength between concrete and reinforcement is assumed not to be affected by corrosion;

therefore, (4), (5) and (7) were used throughout the lifetime of the beam to estimate flexure and shear capacities.

- If a random variable is assumed to be also SV, all variables which depend on that variable were also treated as an SV. For example, (w_c) and (D_{app}) are dependent variables on (f_c'), therefore, they are also SV.
- Although several mechanisms exist, chlorides penetration through the concrete cover in the current case was assumed to happen solely due to diffusion. Furthermore, the presence of cracks (e.g. due to load-induced stresses, shrinkage, or corrosion product expansion) has not been considered in the present analysis and its consideration is beyond the scope of this paper.

6. RESULTS AND DISCUSSION

For both failure modes, flexure and shear, and for each of the two forms of corrosion, general and pitting, the annual reliability indices corresponding to the beam annual failure probabilities were calculated for 100 years of the beam service life (in 5 years' increments).

6.1. Influence of Pitting Corrosion

The influence of pitting corrosion on the safety profile will be discussed in terms of Flexure versus Shear and SV versus NO SV analysis. The results of $\beta(t)$ indicating Flexure, Shear, and Total were produced employing (28), (29), and (30) respectively in (31) and (34).

Figure 10 indicates that the beam reliability decreases with time. This is due to the reduction of the cross-sectional area of flexure and shear reinforcements. For both cases, general and pitting corrosion, the reduction of the beam reliability over time can be seen to be governed by shear rather than by flexure for both spatial and no spatial analysis. Due to their relatively smaller cover depths, as compared to the main flexure reinforcements, shear links are expected to have a shorter T_i period (according to Equation 1) and a higher value of i_{corr} (according to Equation 31). It is therefore expected that shear links are more vulnerable to corrosion attack than flexure reinforcement. Furthermore, the shear links have a smaller diameter which implies that the percentage loss in the cross-sectional area is more prominent in the case of shear

than in the case of flexure. This agrees well with the literature (e.g. Val, 2005) which indicated that the influence of shear failure on the beam reliability increases when higher diameter bars are used for the longitudinal (flexure) reinforcement.

Figure 10 also indicates the severe influence that pitting corrosion can impose on the beam reliability, particularly when the reliability of the beam is governed by the Shear LS. This agrees well with the literature, for example, the results shown in Figure 10 confirm the concluding remarks by Val (2005) who indicated that the reliability of the corroding RC structures may be significantly overestimated if pitting corrosion of the shear links was not considered. It can therefore be concluded that the reduction of the beam shear resistance due to pitting corrosion has a major effect on the reliability of the beam under consideration

6.2. Influence of Spatial Variability

To investigate the influence of considering SV on the safety profile of the beam girder under consideration, results presented in Figure 10 for flexure and shear were re-plotted on a single graph, Figure 11. The first observation can be made from this new figure that SV has no influence on the predicted reliability indices in terms of shear for both cases general and pitting corrosion. This means that the violation of the shear LS was governed by the end support SV element where the induced shear force is expected to be at the peak.

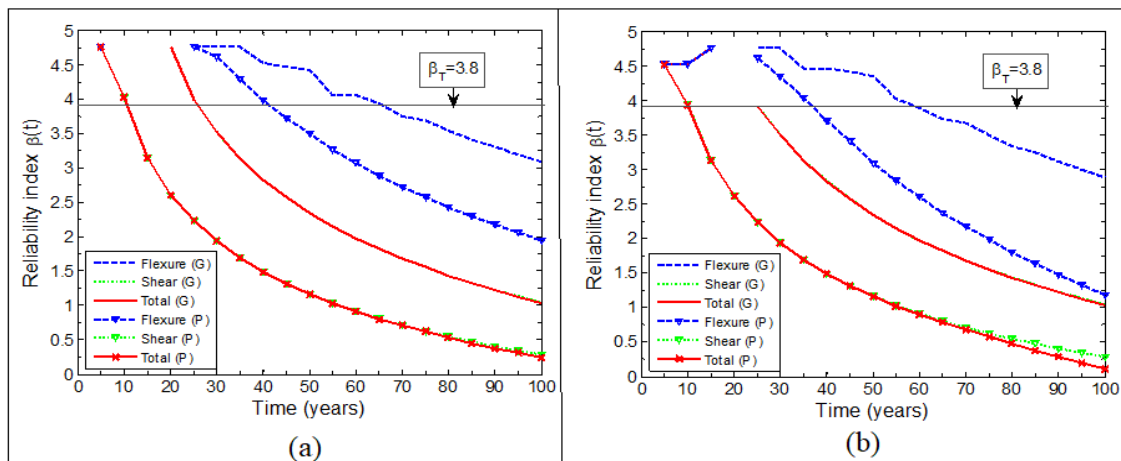


Figure 10: Influence of General (G) and Pitting (P) corrosion on the beam safety profile for (a) No Spatial Variability (NSV) and (b) Spatial Variability (SV)

The second observation which can be made from Figure 11 is that the influence of SV on the beam reliability in terms of flexure is more evident in the case of pitting corrosion than in the case of general corrosion. For example, after 50 years of service, the inclusion of SV has caused the flexure beam reliability predicted in terms of pitting corrosion to decrease by 12% as compared to that predicted when SV was not

considered (NSV). In the case of general corrosion, the decrease in the flexure reliability was only about 2% for the SV when compared to the NSV scenario. It can be concluded therefore that ignoring SV can lead to overestimation of the beam reliability, more evidently in the case of pitting corrosion, when the reliability of the beam is governed by the flexure mode of failure.

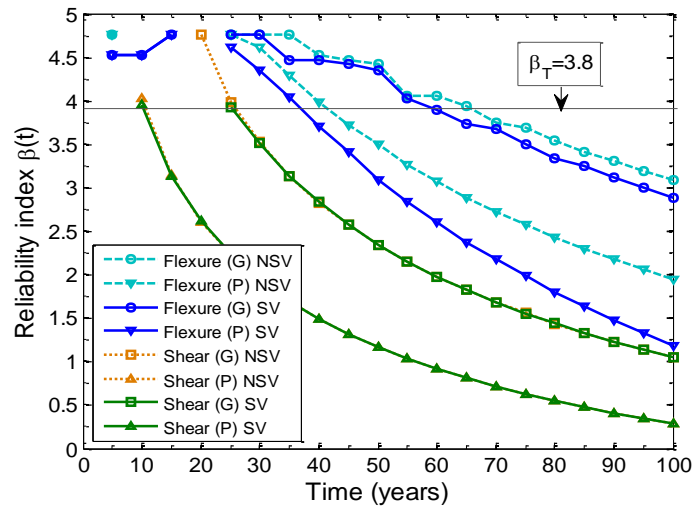


Figure 11: Flexure and Shear reliability for General (G) and Pitting (P) corrosion, considering Spatial variability (SV) and No spatial variability (NSV), Reproduced from Figure 10 (a) and (b)

The reason why the SV influence was more significant in the case of flexure than in the case of shear can be attributed to the fact that the critical zone by which the LS experiences violation is wider for flexure than in the case of shear. For example, for the 31 SV elements, more elements are likely to govern the flexure LS than elements that are likely to govern the shear LS. To support this conclusion, a histogram was constructed, Figure 12, to show the frequency of SV elements that has governed the LS for the two failure modes, flexure, and shear. Figure 12 shows that the governing LS is not always at the mid-span in the case of flexure or at the end support in the case of shear.

However, the figure shows that the mid-span SV element (#16) has governed the LS about 25% of the time. The remaining 75% were shared by all other elements with the element adjacent to the mid-span element having a higher proportion than those further away. Meanwhile, in the case of shear, the end support element (#1) has governed the shear LS about 47% of the time. The remaining SV elements, in this case, governed the LS violation fewer times than that in the case of flexure. This explains that why the influence of SV on the reliability of the beam is expected to be more prominent in the case of flexure than in the case of shear.

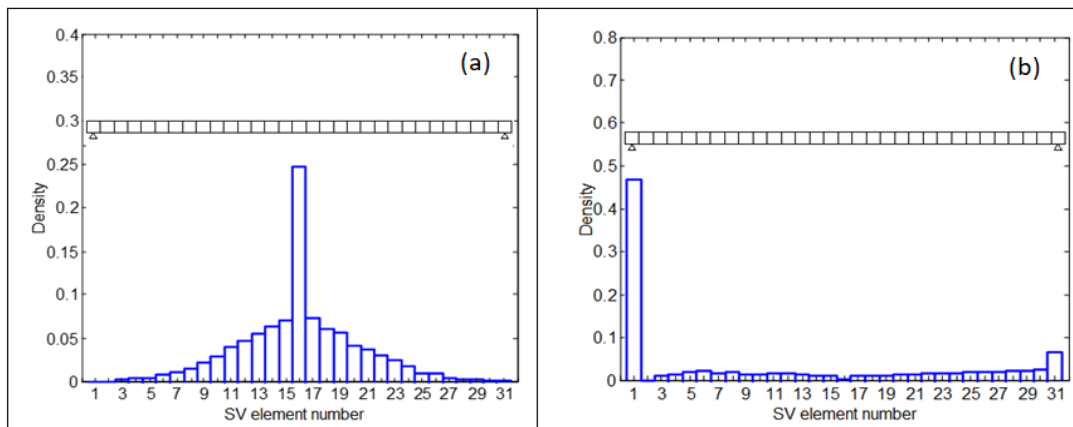


Figure 12: Histogram of SV element which governs the limit state failure after 50 years of service due to pitting corrosion for (a) Flexure (b) Shear

Figure 13 (reproduced from Figure 11) shows the safety profile predicted in terms of the combined (Total) reliability for general (G) and pitting (P) corrosion with the inclusion of SV and without SV (NSV). The figure indicates that the influence of SV is not significant because (as explained earlier) the combined safety profile, in this case, is governed by shear rather than flexure. However, it is evident from

the figure that pitting corrosion has a stronger effect on beam reliability than general corrosion. For example, after 50 years of service, the combined reliability of the beam due to pitting corrosion was 1.16 versus 2.35 due to the general corrosion. Thus, it can be said that after 50 years of service, the reduction in the beam reliability due to pitting corrosion is 51% higher than that caused by general corrosion.

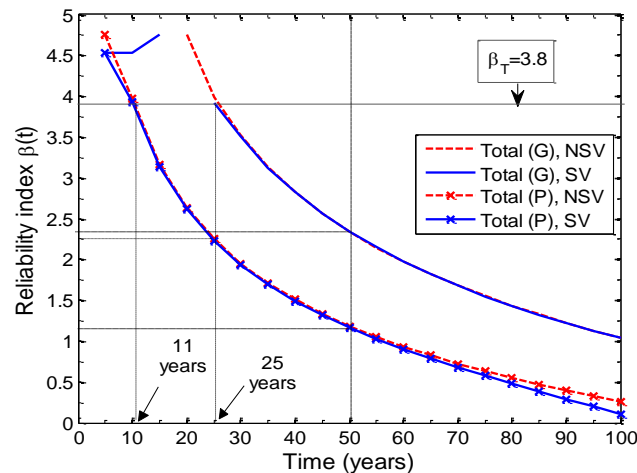


Figure 13: The total reliability (safety profile) is reproduced from Figure 10 for General (G) and Pitting (P) with Spatial Variability (SV) and without Spatial Variability (NSV)

If the safety profile is shown to be governed by pitting corrosion, as in the current case, the assumption which neglects the effect of loss of bond between the reinforcement and concrete as a result of excessive cracking or spalling can therefore be justified. For example, since pitting corrosion is localized, it is less likely to disrupt the concrete cover and hence no reduction is expected for the bond strength around the pits (Val and Melchers, 1997).

6.3. Time for First Repair/Maintenance

If the decision on the time to first repair/maintenance is to be made based on Ultimate Limit State (ULS) and its related target reliability as specified by EC2 (i.e. $\beta_T=3.8$ for Class CC2), the time to first repair/maintenance was found to be about 25 years after the beam construction in the case of general corrosion, Figure 13. When pitting corrosion was considered, the time to first repair/maintenance would be required after only 11 years of the beam construction. In both cases, the beam has failed to maintain its intended design service life (50 years) by a significant margin. The case is more critical when considering pitting corrosion which is in contrast with what some researchers (e.g. Vu and Stewart, 2000) had postulated. The view of the mentioned researchers was that pitting corrosion would not significantly influence the structural capacity of the corroding structure because it is unlikely that many bars will be affected by pitting. The results presented here, Figure 13, have shown that pitting corrosion is more critical than general corrosion from the safety viewpoint. The results presented here indicate that the time to first repair/maintenance of chloride-affected bridge structures should consider the reliability (safety) of the structure (i.e. ULS) and should not only rely on the surface (visual) condition (i.e. Serviceability LS).

7. CONCLUSION

For the two forms of corrosion, general and pitting corrosion, the results showed that pitting

potentially has a far more aggressive effect on the beam reliability than general corrosion. For example, after 50 years of service, the reduction in the beam reliability due to pitting corrosion is 51% greater than that caused by general corrosion.

The results also suggested that pitting corrosion affects shear resistance far more severely than it would affect flexure resistance. For example, after 50 years of service, pitting corrosion has caused the shear resistance to be reduced by 55% when compared to that caused by general corrosion. In the case of flexure, no difference between the reductions caused by both forms of corrosion could be observed. The literature reported that many of today's deteriorating RC bridge structures, including the bridge taken as an example in this study, deteriorate due to corrosion caused by chloride-contaminated water leaking through the deck joints. This means that an intense form of deterioration can take place in parts where high shear stresses are expected (e.g. beam girders at the supports). Therefore, pitting corrosion at locations of high shear stresses can have a severe impact on structure safety. This had led to conclude that the assessment of the safety of RC beams in marine environments should consider the effect of pitting corrosion of shear links on the shear resistance of the beam, otherwise reliability of the beam may be considerably overestimated.

The analysis of this research has shown that SV can be particularly important if the beam reliability was governed by flexure rather than by shear. The influence of SV on the beam reliability was more clear in the case of pitting than in the case of general corrosion. When the beam reliability was governed by the shear LS, SV has no influence.

Results presented in this paper have also indicated that if only the general corrosion was considered, the decision of the time to repair/maintenance intervention can be made based on

the safety criteria of the structure rather than by the traditionally used visual condition criteria. Furthermore, if the performance criteria to be considered for the time to first repair/maintenance decision do not take into account pitting corrosion, the predicted time to first maintenance intervention may be too permissive. These findings strongly point to the necessity of having a bridge management system tool that considers the lifetime safety of the structure as a viable indicator for maintenance and repair interventions.

REFERENCES

1. AASHTO-LRFD bridge design specifications: SI units, American Association of State Highway and Transportation Officials, Washington, D.C, 1994.
2. ACI 209. Prediction of creep, shrinkage and temperature effects: 2. ACI Committee 209, Subcommittee II. In: Draft Report. Detroit: American Concrete Institute, Detroit, USA, 1978.
3. Andrade, C., & Alonso, C. (1996). Corrosion rate monitoring in the laboratory and on-site. *Construction and building materials*, 10(5), 315-328.
4. Barker, R. M., & Jay, P. (1997). Design of highway bridges: based on AASHTO LRFD bridge design specifications, Wiley, New York, USA.
5. Bertolini, L. (2004). Corrosion of steel in concrete: prevention, diagnosis, repair. Wiley-VCH, Weinheim; Cambridge.
6. BS 8110:1. Structural use of concrete. Code of practice for design and construction. British Standard Institute, 1997.
7. Duprat, F. (2007). Reliability of RC beams under chloride-ingress. *Construction and building materials*, 21(8), 1605-1616.
8. EN 1990:2002. Eurocode-Basis for structural design, CEN. European Committee for Standardization, Brussels, 2002.
9. Enright, M. P., & Frangopol, D. M. (1998). Probabilistic analysis of resistance degradation of reinforced concrete bridge beams under corrosion. *Engineering structures*, 20(11), 960-971.
10. Enright, M. P., & Frangopol, D. M. (2000, June). Reliability-based lifetime maintenance of aging highway bridges. In *Nondestructive Evaluation of Highways, Utilities, and Pipelines IV* (Vol. 3995, pp. 4-13). International Society for Optics and Photonics.
11. Eom, J., & Nowak, A. S. (2001). Live load distribution for steel girder bridges. *Journal of Bridge Engineering*, 6(6), 489-497.
12. Frangopol, D. M., Kong, J. S., & Gharaibeh, E. S. (2001). Reliability-based life-cycle management of highway bridges. *Journal of computing in civil engineering*, 15(1), 27-34.
13. Gonzalez, J. A., Andrade, C., Alonso, C., & Feliu, S. (1995). Comparison of rates of general corrosion and maximum pitting penetration on concrete embedded steel reinforcement. *Cement and concrete research*, 25(2), 257-264.
14. Haldar, A., & Sankaran, M. (2000). Probability, reliability and statistical methods in engineering design. Wiley, New York; Chichester.
15. Kenshel, O., & O'Connor, A. (2009). Assessing chloride induced deterioration in condition and safety of concrete structures in marine environments. *European journal of environmental and civil engineering*, 13(5), 593-613.
16. Kenshel, O. (2009). "Influence of spatial variability on whole life management of reinforced concrete bridges." Ph.D. Thesis, Trinity College Dublin, Ireland, 71-103.
17. Kenshel, O. M., O'Connor, A. J., Suleiman, M. F., & Jarushi, F. E. (2021). Role of Spatial Variability in the Service Life Prediction of RC Bridges Affected by Corrosion. *Journal of Civil & Environmental Engineering*, 11(2).
18. Li, Y., Vrouwenvelder, T., Wijnants, G. H., & Walraven, J. (2004). Spatial variability of concrete deterioration and repair strategies. *Structural concrete*, 5(3), 121-129.
19. Liu, Y., & Richard, E. W. (1998). Modeling the time-to-corrosion cracking in chloride contaminated reinforced concrete structures. *ACI Materials Journal*, (95), 675-681.
20. Malioka, V., & Faber, M. (2004). "Modeling of the spatial variability for concrete structures". 2nd International Conference on Bridge Maintenance, Safety and Management (IABMAS), Watanabe, Frangopol and Utsunomiya (eds), A.A. Balkema Publishers, Kyoto, Japan, 18-22.
21. Narayanan, R. S., & Beeby, A. W. (2001). Introduction to Design for Civil Engineers. Spon Press, London.
22. Nowak, A. S., Park, C. H., & Casas, J. R. (2001). Reliability analysis of prestressed concrete bridge girders: comparison of Eurocode, Spanish Norma IAP and AASHTO LRFD. *Structural safety*, 23(4), 331-344.
23. O'Connor, A. J., & Kenshel, O. (2013). Experimental evaluation of the scale of fluctuation for spatial variability modeling of chloride-induced reinforced concrete corrosion. *Journal of Bridge Engineering*, 18(1), 3-14.
24. O'Connor, A. J. (2001). *Probabilistic traffic load modelling for highway bridges* (Doctoral dissertation, Trinity College Dublin).
25. Somo, S., & Hong, H. P. (2006). Modeling error analysis of shear predicting models for RC beams. *Structural Safety*, 28(3), 217-230.
26. Stewart, M. G. (1997). Time-dependent reliability of existing RC structures. *Journal of Structural Engineering*, 123(7), 896-902.
27. Stewart, M. G., & Mullard, J. A. (2007). Spatial time-dependent reliability analysis of corrosion damage and the timing of first repair for RC structures. *Engineering structures*, 29(7), 1457-1464.
28. Stewart, M. G., & Suo, Q. (2009). Extent of spatially variable corrosion damage as an indicator

- of strength and time-dependent reliability of RC beams. *Engineering Structures*, 31(1), 198-207.
29. Stewart, M. G. (1997). Concreting workmanship and its influence on serviceability reliability. *Materials Journal*, 94(6), 501-509.
30. Tabsh, S. W., & Nowak, A. S. (1991). Reliability of highway girder bridges. *Journal of structural engineering*, 117(8), 2372-2388.
31. Val, D. V., & Melchers, R. E. (1997). Reliability of deteriorating RC slab bridges. *Journal of structural engineering*, 123(12), 1638-1644.
32. Val, D. V., Stewart, M. G., & Melchers, R. E. (1998). Effect of reinforcement corrosion on reliability of highway bridges. *Engineering structures*, 20(11), 1010-1019.
33. Val, D. (2005). "Effect of pitting corrosion on strength and reliability of reinforced concrete beams." Proceedings of the ninth international conference on structural safety. ICOSSAR, A.A. Balkema, Rotterdam, 257-264.
34. Vanmarcke, E. (1983). Random fields: analysis and synthesis, MIT Press, Cambridge, Mass; London.
35. Vu, K. A., & Stewart, M. G. (2005). Predicting the likelihood and extent of reinforced concrete corrosion-induced cracking. *Journal of structural engineering*, 131(11), 1681-1689.
36. Vu, K. A. T., & Stewart, M. G. (2000). Structural reliability of concrete bridges including improved chloride-induced corrosion models. *Structural safety*, 22(4), 313-333.
37. Chu-Kia, W., & Charles, S. (2002). Reinforced concrete design. John Wiley & Son's, Inc., New York, USA.